

## Effect of Al<sub>2</sub>O<sub>3</sub> addition on the microstructure and mechanical properties of the electroformed Ni/Al<sub>2</sub>O<sub>3</sub> composite stencil masks

Ji Cheol Kim<sup>a</sup>, Geun Chul Park<sup>a</sup>, Soo Min Hwang<sup>a</sup>, Jun Hyuk Choi<sup>a</sup>, Tae Woong Kim<sup>a</sup>, Jun Hyung Lim<sup>a,\*</sup>,  
Keun Song<sup>b</sup> and Jinho Joo<sup>a,\*</sup>

<sup>a</sup>School of Advanced Materials Science and Engineering, Sungkyunkwan University, Suwon 440-746, Korea

<sup>b</sup>Dept. of Application of Advanced Materials, Suwon Science College, Suwon 445-742, Korea

Monolithic and composite Ni/Al<sub>2</sub>O<sub>3</sub> stencil masks were produced using an electroforming process and photolithography technology and evaluated the effect of co-deposited Al<sub>2</sub>O<sub>3</sub> content on microstructure, texture, surface roughness, and mechanical properties. For the composites,  $\alpha$ -Al<sub>2</sub>O<sub>3</sub> powders with a particle size of 300 nm were added to the electrolyte, and the content of co-deposited Al<sub>2</sub>O<sub>3</sub> in the specimen increased as its concentration in solution increased. For all samples, the Ni phase was crystallized and the Ni (002) planes formed parallel to the surface. On the other hand, the (200) texture became weaker with increasing Al<sub>2</sub>O<sub>3</sub> content. Mechanical properties improved with increasing Al<sub>2</sub>O<sub>3</sub> content. Specifically, the 30.35 vol% co-deposited composite exhibited a higher hardness (394 Hv) and lower volume loss (0.321 mm<sup>3</sup>) than the pure Ni mask (231 Hv and 2.106 mm<sup>3</sup>). These improvements may be due to the strengthening mechanisms such as the dispersion hardening and formation of hard contact points of Al<sub>2</sub>O<sub>3</sub> in the Ni matrix for the counterpart during sliding.

**Key words:** Electroforming, Hardness, Ni-Al<sub>2</sub>O<sub>3</sub> composite, Stencil mask, Wear properties.

### Introduction

Flip chip bonding via screen printing is widely used in various electronic packaging techniques to fabricate input/output gates, which transfer an electrical signal between the substrate and chips by forming solder bumps. Because solder bumps provide a conductive pad without Au wires and shorten the distance between the package and chips, this technique has the advantage of establishing connections among sophisticated structures on printed circuit boards (PCBs) [1]. Stencil masks are finely patterned metal plates used to form solder bumps by squeezing solder paste through holes in the mask. Thus, it is essential that such masks have fine holes of uniform shape, a smooth surface, and excellent mechanical properties for a long service life.

Recently, the electroforming process has been used to fabricate nickel (Ni) stencil masks with fine holes and fine pitch (< 50  $\mu$ m) using photolithography techniques to replace conventional stainless steel masks made by chemical or laser etching methods, both of which suffer from the drawbacks of reduced hole and pitch size [2]. On the other hand, the hardness and wear properties of electroformed Ni mask need to be improved further such that they can endure the frictional stress from the reciprocating motion of solder paste squeezers. Improved mechanical properties of electroformed Ni plates can be

achieved by either modification of the monolithic microstructures or the development of composite microstructures with a second phase addition. Substantial research has been conducted to understand the role of current density, pH, and electrolyte composition in monolithic Ni plates. Several groups have added hard particles such as SiC [3], TiO<sub>2</sub> [4], diamond [5], ZrO<sub>2</sub> [6], Al<sub>2</sub>O<sub>3</sub> [7], and WC [8], and so on, to the Ni and reported the effect of these particles (i.e., type, size, content) on microstructure, strength, and hardness of composite Ni plates. However, asystematic study of the role of particle content on texture and wear properties has not been completed.

In the present study, we fabricated both monolithic and composite Ni masks by adding various amount of Al<sub>2</sub>O<sub>3</sub> in electrolyte (3-150 g/l) using an electroforming process and evaluated the co-deposited Al<sub>2</sub>O<sub>3</sub> content, texture, and surface morphology of composite Ni masks. In addition, mechanical properties such as hardness and wear resistance were characterized.

### Experimental Procedure

Both pure and composite Ni stencil masks were fabricated by the electroforming process with the photolithographic technique. Before the electroforming process, additive patterns were introduced onto a stainless steel (SUS 304) plate with dimensions of 100 mm  $\times$  100 mm  $\times$  0.1 mm through a photolithography process. Dry photoresist film lamination, photo masking, exposure, and development procedures were used in this process. The minimum diameter and pitch

\*Corresponding author:  
Tel : +82-31-290-7385  
Fax: +82-31-299-4749  
E-mail: jinho@skku.edu

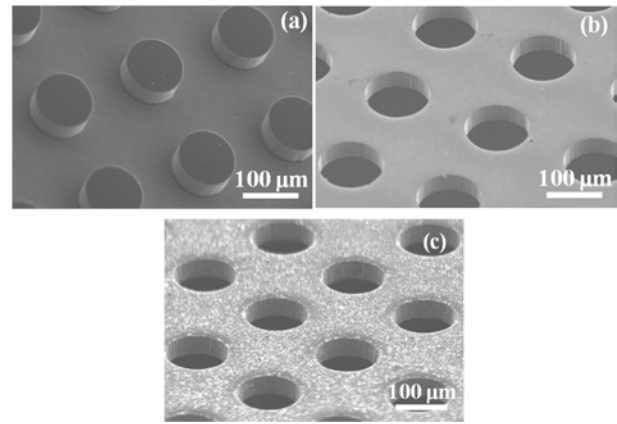
**Table 1.** Photolithography and electroforming process conditions.

Photolithography conditions	
Laminating conditions	
DFR (Dry Film Resist)	KM-1150 (Kolon)
Roll pressure/Temp. of roll	0.4 MPa/110 °C
Laminating speed	2 m/min
Exposure conditions	
Distance between substrate and source	200 mm
Does	80 mJ/cm <sup>2</sup>
Power/ Time	500 W/131 sec
Development conditions	
Solution	Na <sub>2</sub> CO <sub>3</sub> (1 wt.%)
Temp./ Time	50 °C/1 h
Electroforming conditions	
Electrolyte	
Ni·(NH <sub>2</sub> SO <sub>3</sub> ) <sub>2</sub> · 4H <sub>2</sub> O	500 ml/l
H <sub>3</sub> BO <sub>3</sub>	45 g/l
NiCl	25 g/l
α-alumina (300 nm)	0-150 g/l
Electroforming	
Temperature	50 °C
pH	4
Current density	DC-1 A/dm <sup>2</sup>
Forming time	4 h

of the additive pattern were 100 and 130 μm, respectively, and the remaining photoresist film was stripped with a NaOH solution. Electroforming was then performed on the additive patterned SUS plate, whereby the plate was used as the cathode and crown-type Ni balls in a titanium basket were used as the anode.

The electrolyte solutions consisted of Ni-sulfamate, boric acid, and Ni-chloride in distilled water. α-Al<sub>2</sub>O<sub>3</sub> powders with a particle size of 300 nm were added to the electrolyte to fabricate co-deposited Ni-Al<sub>2</sub>O<sub>3</sub> composite masks. The concentrations of Al<sub>2</sub>O<sub>3</sub> in the electrolyte bath were 0, 3, 6, 10, 30, 90, and 150 g/l, hereafter denoted as pure, 3, 6, 10, 30, 90, and 150 g/l specimens, respectively. To de-flocculate and suspend the powders uniformly, solutions were subjected to ultrasonic treatment for 10 min and then stirred with an agitator at a rotation speed of 360 rpm. The electrolyte was kept at 50 °C and its pH was set to 4.0. The current density and plating time were DC-1 A/cm<sup>2</sup> and 4 hours, respectively. Strain-free and uniform masks with a thickness of 40 μm were obtained after optimizing the processing variables. Table 1 shows the photolithography and electroforming process conditions.

Phase identification was performed by X-ray diffraction (XRD, Bruker-AXS). The microstructures and surface

**Fig. 1.** SEM micrographs of the (a) positively patterned photoresist film on SUS and of the (b) pure Ni and (c) 30 g/l stencil masks.

roughness were observed by scanning electron microscopy (SEM, XL-30, ESEM-FEG) and atomic force microscopy (AFM, Hitachi-1000) in contact mode with a detection area of 20 μm × 20 μm, respectively. The co-deposited Al<sub>2</sub>O<sub>3</sub> content was analyzed using an energy dispersive spectrometer (EDS). Microhardness was determined using a Vicker's micro-hardness indenter with a load of 200 g<sub>f</sub> for 10 sec. The final hardness was based on the average of ten measurements. Friction and wear behavior was assessed using a reciprocating ball-on-disk method at room temperature under dry sliding conditions, and an AISI-52100 steel ball (8 mm in diameter) was used as the counter body. All tests were performed under a load of 150 g<sub>f</sub>, a sliding speed of 0.2 m/s, a total friction distance of 2,000 m, and a track radius of 2 cm. The volume loss of the specimens and balls was calculated using the mean wear area determined by SEM. The friction coefficient and sliding time were recorded automatically during the test.

## Results and Discussion

The pure and composite Ni stencil masks with the desired 100 μm diameter and 130 μm pitch geometry were successfully fabricated after optimizing the photolithography and electroforming processes. Fig. 1 shows the SEM micrographs of the positively patterned photoresist film on SUS and of the pure Ni and Ni/Al<sub>2</sub>O<sub>3</sub> composite (30 g/l) stencil masks. The shape and dimensions of the remaining positive patterns on the photoresist films were very close to those of the holes in the Ni mask (> 1 μm tolerance limit). The mask images showed that the surface was smooth and strain-free, and that the holes were round with uniform sidewall geometry. Similarly, the vertical surfaces of the inner holes in both masks were smooth and dense without any microcracks. The white spots on the surface of the composite masks were Al<sub>2</sub>O<sub>3</sub>, and there was no distinct difference in the shape of holes between the pure and composite mask.

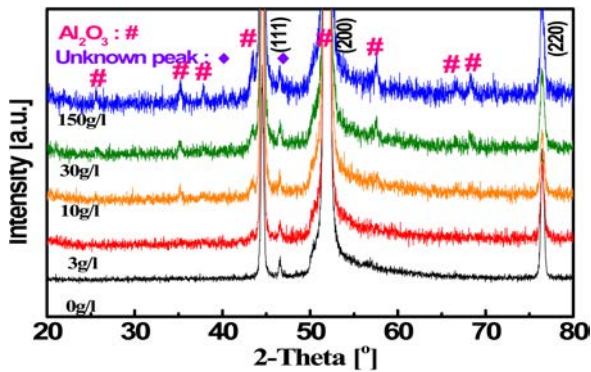


Fig. 2. XRD patterns of the monolithic and composite specimens.

Fig. 2 shows the XRD patterns of pure and composite Ni plates. All specimens consisted mainly of the Ni phase, with a Ni-Ti associated peak observed at  $46.56^\circ$  [9], which was probably the result of using a Ti basket in the electrolyte bath.  $\text{Al}_2\text{O}_3$  peaks began to appear in the 10 g/l sample, the intensity of which increased slightly up to the 150 g/l specimen, indicating that the  $\text{Al}_2\text{O}_3$  particles were co-deposited and their content increased as the concentration of  $\text{Al}_2\text{O}_3$  in solution increased. It was also noted that the Ni phase was crystallized and the Ni (002) and (111) planes formed parallel to the surface of the specimens for all samples, whereas the relative intensities of the major peaks differed from each other. Electroplated metals are known to have a largely amorphous structure or a non-textured crystalline structure, depending on the processing conditions [10]. However, textured Ni developed when the processing variables were optimized, as shown in Table I. The XRD analysis was used to evaluate the degree of texturing from the ratio of the X-ray peak intensity of the (002) plane to the (111) plane of Ni, i.e.,  $I_{(002)}/\{I_{(002)} + I_{(111)}\}$ . For the pure sample, this ratio was 0.967, and decreased to 0.927, 0.881, 0.783, and 0.753 for the 3, 10, 30, and 150 g/l samples, respectively, suggesting that the texture was reduced as the  $\text{Al}_2\text{O}_3$  content increased. This result was acceptable because the presence of a second phase/particle can generally interrupt the formation of texture.

Fig. 3 shows the top views of an SEM image of both pure and composite specimens. We observed that the content of co-deposited  $\text{Al}_2\text{O}_3$  increased as its concentration in solution increased, the relationship of which is plotted in Fig. 3(f). For the 3 g/l specimen, the content was 13.02 vol% and it rapidly increased to 19.1 and 23.1 vol% for the 6 and 10 g/l specimens, respectively, but increased only slightly thereafter to 25.11, 28.55, and 30.35 vol% for the 30, 90, and 150 g/l specimens, respectively. Hereafter, the 3, 6, 10, 30, 90, and 150 g/l specimens are also denoted as the 13.0, 19.1, 23.1, 25.1, 28.6, and 30.4 vol% specimens, respectively.

Wang et al. reported that 30 nm-sized  $\text{Al}_2\text{O}_3$  particles are positively charged in electrolyte [11]. Therefore, it is thought that the suspended  $\text{Al}_2\text{O}_3$  particles in our

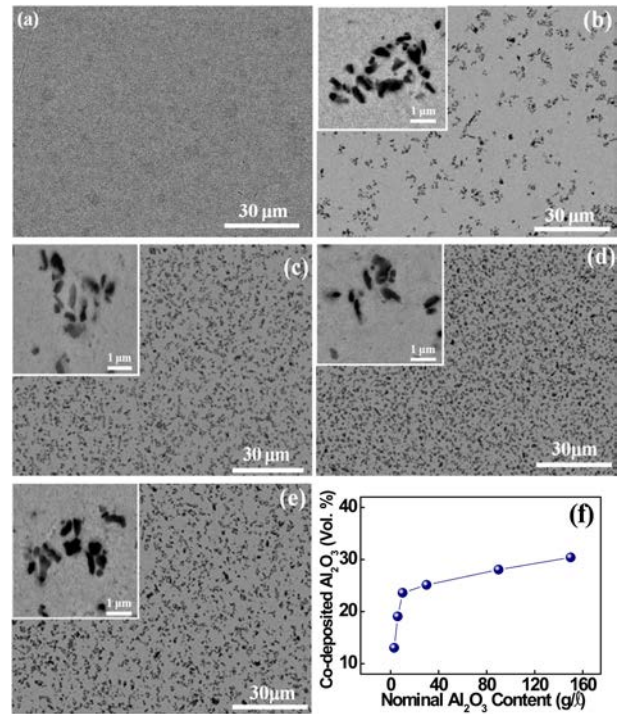


Fig. 3. SEM micrographs of (a) pure, (b) 3 g/l, (c) 10 g/l, (d) 30 g/l, and (e) 150 g/l specimens and (f) the co-deposited  $\text{Al}_2\text{O}_3$  content.

study were adsorbed onto the electrode by two-step adsorption mechanism [12]. In the first step, the stable particles are loosely adsorbed on the cathode and they are in equilibrium with the particles in suspension. The particles are still surrounded by adsorbed ions and solvent molecules. For the second step, this ion/molecules screen is broken through so that a strong electrochemical adsorption of particles onto the cathode takes place. The particles are bound to the grown surface and are consequently embedded in the Ni deposit. For this model, Gugliemi et al. derived the following equation [12];

$$\frac{C}{\alpha} = \frac{Mi_0}{nF\rho_m v_0} \exp(A-B)\eta \left( \frac{1}{k} + C \right) \quad (1)$$

where  $C$  is the concentration of suspended particles and  $\alpha$  is the volume fraction in the deposit.  $M$  is the atomic weight of the electrodeposited metal,  $i_0$  is the exchanging current density,  $n$  is the valence of the electrodeposited metal,  $F$  is the Faraday constant,  $\rho_m$  is the density of electrodeposited metal,  $\eta$  is the overpotential of electrode reaction, and  $k$  is Langmuir adsorption constant. In addition, the parameters  $v_0$  and  $B$  are related to particles deposition, and both play a symmetrical role with parameters  $i_0$  and  $A$  related to metal deposition. They reported that  $C/\alpha$  linearly increased with increasing concentration of suspended particles in the electrolyte. In our study, as the concentration of  $\text{Al}_2\text{O}_3$  in the solution increased, the amount of  $\text{Al}_2\text{O}_3$  that could reach to the diffusion boundary layer increased, resulting in increased co-deposition. On the other hand, further increases in the

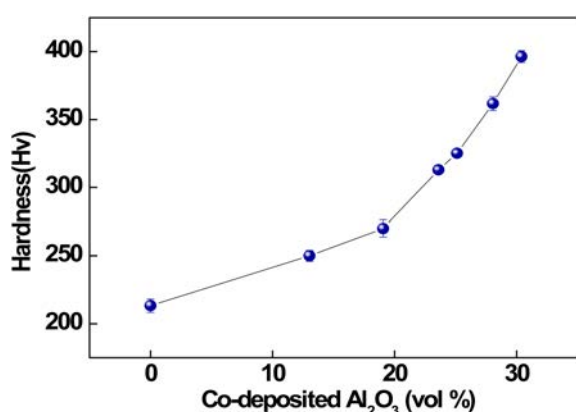


Fig. 4. Dependence of microhardness on the co-deposited Al<sub>2</sub>O<sub>3</sub> content in solution.

Al<sub>2</sub>O<sub>3</sub> concentration in the solution caused increased the probability of collision and sputtering of the particles being absorbed on the surface of the cathode, and thus caused disruption at the cathode. This is believed to be the cause of the smaller increase in the Al<sub>2</sub>O<sub>3</sub> content for the 30-150 g/l specimens compared to the others.

In addition, the magnified images (insets of Figs. 3(b)-(e)) show that the Al<sub>2</sub>O<sub>3</sub> particles were not uniformly dispersed, but rather were aggregated. For the 13.0 vol% specimen, the size of the co-deposited particles was in the range of 0.2-0.9 μm, with 20-30 particles forming a cluster, and hence, the surface of the pure Ni region was clearly distinguishable from that of the clustered region. This clustering likely occurred because the particles tended to flocculate to each other in order to lower the surface energy in the solution [13]. Thus, addition of an appropriate surfactant is expected to eliminate or minimize this segregation [14, 15]. The clusters decreased in size as the Al<sub>2</sub>O<sub>3</sub> content increased, with five to ten particles forming a cluster in the 30.4 vol% specimen. Because the probability of collision increases with increasing Al<sub>2</sub>O<sub>3</sub> content as noted above, repeated flocculation and dispersion of the particles reduced the level of aggregation in the solution, which might have been the reason for this specimen having a smaller cluster size [16].

Surface roughness was measured by AFM (images were not shown here). The RMS values were in the range of 129.0 nm to 186.9 nm for all samples and increased with increasing Al<sub>2</sub>O<sub>3</sub> content. This increase is thought to have resulted from the co-deposited Al<sub>2</sub>O<sub>3</sub> particles on or near the surface. As the Al<sub>2</sub>O<sub>3</sub> content increased, the number of particles protruding from the surface increased, thereby increasing the surface roughness.

Fig. 4(a) illustrates the dependence of hardness on co-deposited Al<sub>2</sub>O<sub>3</sub> content. The hardness of pure Ni specimens was 213.3 Hv, the value of which increased nearly monotonically with increasing Al<sub>2</sub>O<sub>3</sub> content, suggesting a close relationship. The hardness values of the 13.0, 19.1, 23.1, 25.1, 28.6, and 30.4 vol% Al<sub>2</sub>O<sub>3</sub> co-deposited specimens were 251.0, 273.0, 312.9, 325.1, 361.6, and 396.4 Hv, respectively. As the co-

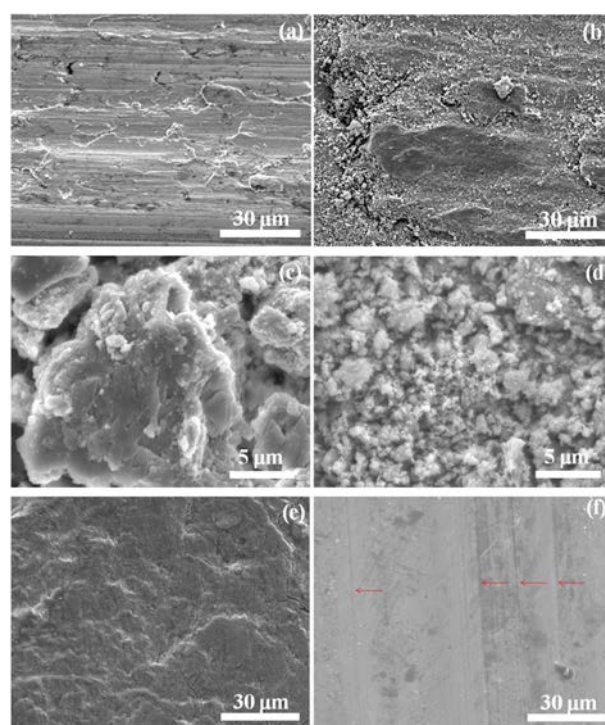
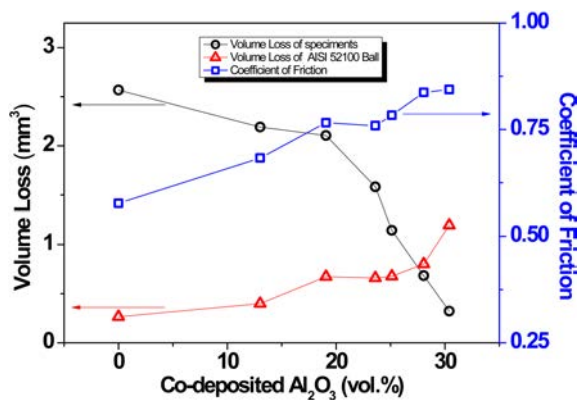


Fig. 5. SEM micrographs of (a) the worn surface of the specimen, (b) its debris, and (c) the worn surface of the counterpart ball for the pure specimen. Panels (d-f) correspond to those for the 150 g/l specimen, respectively.

deposited Al<sub>2</sub>O<sub>3</sub> content increased, the distance between the clusters decreased. Specifically, the distance was 15.2 μm for the 13.0 vol% specimen and gradually decreased with Al<sub>2</sub>O<sub>3</sub> content to 6.2 μm in the 30.4 vol% specimen: the variation of the distance showed opposite trend to that of hardness. The presence of hard particles in a Ni matrix can hinder dislocation movement and plastic deformation. In addition, we expect that the particles obstructed grain boundary motion, leading to grain refinement. Thus, the improvement in hardness is attributed to strengthening mechanisms such as dispersion hardening and grain size strengthening.

The ball-on-disc method under dry sliding conditions was employed to evaluate friction and wear properties. Fig. 5 shows the worn surface for pure and 30.4 vol% specimens as well as their respective wear debris and the worn surface of the counterpart ball. The pure Ni specimen had many cracks and a multi-layered structure along the entire surface (Fig. 5(a)), indicating that the surface was scuffed, deformed, and then chipped away in a plate shape. This type of surface is observed in cases of adhesive wear in which continuous compressive and tensional stresses induce significant dislocations, which lead to a brittle surface vulnerable to crack initiation and propagation along the hardened surface, ultimately resulting in plate-shaped wear [17, 18]. The debris from the pure Ni consisted of plate-shaped particles (Fig. 5(c)) and the counterpart ball (Fig. 5(e)) was also worn in adhesive mode. For the 30.4 vol.% Al<sub>2</sub>O<sub>3</sub> co-deposited specimens, the worn



**Fig. 6.** Variations in the volume loss of the specimen, and ball and friction coefficient after the wear test with the co-deposited Al<sub>2</sub>O<sub>3</sub> content in solution.

surface and debris exhibited a partly multi-layer structure and plate shape, respectively, as shown in Figs. 5 (b) and (d), and these features are consistent with adhesive wear mode. Interestingly, the debris and plate-shaped wear was decreased compared to that of the pure specimen. This is probably because the Al<sub>2</sub>O<sub>3</sub> particles restricted dislocation movement, plastic flow, as well as the formation and propagation of cracks. The worn surface of the counterpart ball (Fig. 5(f)) was flat and had several linear grooves indicated by arrows, which is a typical morphology resulting from abrasive wear. This type of morphology generally occurs when a hard surface slides against and cuts grooves into a softer surface [19]. We assumed that the presence of Al<sub>2</sub>O<sub>3</sub> particles affected the wear mode because they have a higher hardness than the ball. Therefore, we expected that the Al<sub>2</sub>O<sub>3</sub> content have influence on the friction coefficient in the composite specimen.

Fig. 6 shows variations in the volume loss of the specimen and ball and the friction coefficients after the wear test. The volume loss (wear volume, V) of the specimen decreased while that of the ball increased as the co-deposited Al<sub>2</sub>O<sub>3</sub> content increased. These variations were attributed to the difference in hardness between the specimen and counterpart ball. In addition, the friction coefficient increased with increasing Al<sub>2</sub>O<sub>3</sub> content. Specifically, the friction coefficient of the pure specimen was 0.576, which increased to 0.77, 0.76, 0.78, 0.84, and 0.84 for the 13.0, 19.1, 23.1, 25.1, 28.6, and 30.4 vol% Al<sub>2</sub>O<sub>3</sub> co-deposited specimens. This variation had a similar trend to that of hardness with respect to increasing Al<sub>2</sub>O<sub>3</sub> content. The improved friction coefficient and hardness of the composite were likely originated from the presence of the reinforced particles. As the Al<sub>2</sub>O<sub>3</sub> content increased, more Al<sub>2</sub>O<sub>3</sub> particles protruded on the surface and increased the contact points for the counterpart during sliding, leading to higher friction coefficients for the composites. This result is opposite to that observed with monolithic materials in which the friction coefficient is generally inversely proportional to hardness [20, 21]. These

composite specimens have superior hardness and wear resistance compared to pure specimens, and thus may provide a higher reliability and a longer service life.

## Conclusions

We fabricated composite Ni/Al<sub>2</sub>O<sub>3</sub> stencil masks by an electroforming process with a photolithography technique and evaluated the effects of Al<sub>2</sub>O<sub>3</sub> content on microstructure, texture, surface roughness, and mechanical properties. For all samples, the Ni phase was crystallized and the Ni (002) planes formed parallel to the surface, whereas the (200) texture became weaker as the Al<sub>2</sub>O<sub>3</sub> content increased. Microstructure analyses showed that the co-deposited Al<sub>2</sub>O<sub>3</sub> content increased monotonically up to the 10 g/l specimen, and increased slightly thereafter. In addition, the co-deposited particles were clustered and the size of the cluster decreased with increasing Al<sub>2</sub>O<sub>3</sub> content, which was likely due to collision of powders during the electroforming process. The presence of co-deposited Al<sub>2</sub>O<sub>3</sub> degraded the surface roughness and improved the hardness and friction coefficient while reducing wear volume. The improved hardness and wear resistance were attributed to strengthening mechanisms such as dispersion hardening and formation of hard contact points of Al<sub>2</sub>O<sub>3</sub> in the Ni matrix for the counterpart during sliding.

## References

1. P.-S. Chao, J.-T. Huang, H.-J. Hsu, S.-H. Shih, *Microelectron. Eng.* 84 (2007) 71.
2. J. H. Lim, EC Park, J Joo and S-B Jung, *J. Electrochem. Soc.* 156 [3] (2009) 112.
3. H-K Lee, H-Y Lee, J-M Jeon, *Surf. Coat. Technol.* 201 (2007) 4717.
4. D. Thiemig, A. Bund, *Surf. Coat. Technol.* 202 (2008) 2984.
5. T.-J. Chen, Y.-C. Chiou, R.-T. Lee, *International Journal of Machine Tools & Manufacture* 49 (2009) 477.
6. W. Wang, F.-Y. Hou, H. Wang, H.-T. Guo, *Scripta. Mater.* 53 (2005) 618.
7. Q. Feng, T. Li, H. Yue, K. Qi, F. Bai, J. Jin, *Appl. Surf. Sci.* 254 (2008) 2268.
8. M. Stroumbouli, P. Gyftou, E.A. Pavlatou, N. Spyrellis, *Surf. Coat. Technol.* 195 (2005) 332.
9. ASTM JCPDS file 75-0878.
10. W. Chen, W. Gao, *Electrochim. Acta.* 55(2010)6871.
11. S.-C. Wang, W.-C.J. Wei, *Mater. Chem. Phys.* 78(2003) 580.
12. N. Gugliemi, *J. Electrochem. Soc.* 119 (1972) 1012.
13. W. Wang, J.C.T. Kwak, *Colsurfa. A* 156 (1999) 110.
14. C.R. Evanko, D.A. Dzombak, J.W. Novak, *ColsurfaA* 110 (1996) 233.
15. J.J. Lopata, K.M. Werts, J.F. Scamehorn, J.H. Harwell, B.P. Grady, *J. Colloid. Interf. Sci.* 342 (2010) 426.
16. S.W. Banovic, K. Barmak, A.R. Marder, *J. Mater. Sci.* 34 (1999) 3211.
17. S. Hogmark, O. Vingsbo, *Wear* 38 (1976) 359.
18. E.F. Finkin, *J. Mater. Eng. Appl.* 1(1979) 161.
19. E.F. Finkin, *Wear* 21 (1972) 113.
20. H. Gul, F. Kylc, S. Aslan, A. Alp, H. Akbulut, *Wear* 267 (2009) 990.
21. J.M. Challjzn and P.L.B. Oxley, *Wear* 111 (1986) 288.